Strong energy–momentum dispersion of phonon-dressed carriers in the lightly doped band insulator $SrTiO_3$

2010 New J. Phys. 12 023004

(http://iopscience.iop.org/1367-2630/12/2/023004)

New Journal of Physics
The open-access journal for physics

Strong energy–momentum dispersion of phonon-dressed carriers in the lightly doped band insulator $SrTiO_3$

W Meevasana[1,2,3,4,12], X J Zhou[5], B Moritz[2], C-C Chen[1,2], R H He[1,2], S-I Fujimori[6], D H Lu[2], S-K Mo[1,7], R G Moore[2], F Baumberger[3], T P Devereaux[2], D van der Marel[8], N Nagaosa[9,10], J Zaanen[11] and Z-X Shen[1,2]

[1] Departments of Physics and Applied Physics, Stanford University, CA 94305, USA
[2] Stanford Institute for Materials and Energy Sciences, SLAC National Accelerator Laboratory, 2575 Sand Hill Road, Menlo Park, CA 94025, USA
[3] School of Physics and Astronomy, University of St. Andrews, North Haugh, St. Andrews, Fife KY16 9SS, UK
[4] Synchrotron Light Research Institute, Nakhon Ratchasima 30000, Thailand
[5] Institute of Physics, Chinese Academy of Sciences, Beijing 100190, People's Republic of China
[6] Synchrotron Radiation Research Unit, Japan Atomic Energy Agency, Mikazuki, Hyogo 679-5148, Japan
[7] Advanced Light Source, Lawrence Berkeley National Lab, Berkeley, CA 94720, USA
[8] Département de Physique de la Matière Condensée, Université de Genève, quai Ernest-Ansermet 24, CH1211, Genève 4, Switzerland
[9] Department of Applied Physics, The University of Tokyo, Bunkyo-ku, Tokyo 1138656, Japan
[10] Cross-Correlated Materials Research Group (CMRG), ASI, RIKEN, Wako 351-0198, Japan
[11] The Instituut-Lorentz for Theoretical Physics, Leiden University, Leiden, The Netherlands
E-mail: wm14@st-andrews.ac.uk

New Journal of Physics **12** (2010) 023004 (11pp)
Received 10 October 2009
Published 3 February 2010
Online at http://www.njp.org/
doi:10.1088/1367-2630/12/2/023004

[12] Author to whom any correspondence should be addressed.

Abstract. Much progress has been made recently in the study of the effects of electron–phonon (el–ph) coupling in doped insulators using angle-resolved photoemission (ARPES), yielding evidence for the dominant role of el–ph interactions in underdoped cuprates. As these studies have been limited to doped Mott insulators, the important question arises as to how this compares with doped band insulators where similar el–ph couplings should be at work. The archetypical case is that of perovskite $SrTiO_3$ (STO), well known for its giant dielectric constant of 10 000 at low temperatures, exceeding that of La_2CuO_4 by a factor of 500. Based on this fact, it has been suggested that doped STO should be the archetypical bipolaron superconductor. Here we report an ARPES study from high-quality surfaces of lightly doped STO. In comparison to lightly doped Mott insulators, we find the signatures of only moderate el–ph coupling; a dispersion anomaly associated with the low-frequency optical phonon with a $\lambda' \sim 0.3$ and an overall bandwidth renormalization suggesting an overall $\lambda' \sim 0.7$ coming from the higher frequency phonons. Furthermore, we find no clear signatures of the large pseudogap or small-polaron phenomena. These findings demonstrate that a large dielectric constant itself is not a good indicator of el–ph coupling and highlight the unusually strong effects of the el–ph coupling in doped Mott insulators.

Contents

1. Introduction

The notion that carriers doped into insulators get dressed by lattice deformations has been around for a long time [1, 2]. A recent development is that this polaron formation can be studied experimentally using angle-resolved photoemission (ARPES), yielding more direct information on the physics than classical transport and optical spectroscopic methods. Especially when the carrier density is small but finite, where a controlled theoretical framework is lacking, ARPES has been quite revealing. The case has been made that lightly doped cuprates fall victim to small-polaron formation (strong interacting case) that is vulnerable to self-trapping by impurities [3, 4]; in undoped cuprates, the spectral functions reveal Frank–Condon-type broad humps caused by the coupling to multiple phonons, and only when doping is increased does a well-defined quasi-particle (QP) peak start to emerge [3, 4]. Another recent ARPES revelation is found in the context of highly doped manganites in the colossal magnetoresistance regime. At high temperatures ARPES reveals the Frank–Condon humps signaling small polarons, while upon lowering temperature small pole-strength QP peaks appear in addition, indicating that a coherent Fermi liquid is formed from the microscopic polarons [5].

Both manganites and cuprates are doped Mott insulators and no modern ARPES information is available on polaron physics in the simpler doped band insulators. We therefore decided to focus on the classic $SrTiO_3$ (STO) doped band insulator. STO is known to have an exceptionally high static dielectric constant on the order of 10^4 at low temperatures [6]. Superconductivity can be induced by electron doping with O, Nb or La [7, 8] over a narrow range of low carrier concentrations between $\sim 10^{19}$ and $\sim 10^{20}\,\mathrm{cm}^{-3}$. Optimal T_c is typically 0.2–0.3 K but can reach up to 1.2 K [9], which is surprisingly high for such low carrier concentrations. It has been speculated that this is due to the formation of bipolarons [10]. However, whether large or small polarons actually exist in STO depends on the relevant length scale for the electron–phonon (el–ph) couplings.

The case was made in a recent optical study by van Mechelen *et al* that el–ph coupling is actually not very strong [11]. ARPES is, however, more direct in revealing the strength of coupling to specific phonons. With this technique we arrive at the conclusion that small polarons are not formed in STO and that el–ph coupling acts in a perturbative way.

2. Methods and materials

The samples investigated here are $La_xSr_{1-x}TiO_{3+\delta}$ (Crystal Base Co., Japan) at nominal dopings of $x = 0.01$ ($T_c \sim 0.2$ K) and $x = 0.05$ (non-superconducting) [8] while the actual doping levels at the surface are slightly different due to oxygen vacancies. We obtain high-quality surfaces by cleaving along guiding lines at $T = 10$ K and measure at the same temperature. This new technique results in significantly flatter surfaces than when fracturing or scraping STO. This was found to substantially improve the quality of ARPES data and enable us to see a clear QP band dispersion and dispersion anomaly, which have not been seen in previous measurements [12]–[14].

ARPES data were collected on a Scienta-4000 analyzer at the Stanford Synchrotron Radiation Laboratory, Beamline 5–4, and the Advanced Light Source (ALS), Beamline 10.0.1, with photon energies between 18 and 90 eV and a base pressure of $<4 \times 10^{-11}$ Torr. Samples were cleaved *in situ* along the (001) plane at the measurement temperature, $T = 10$ K. A sharp (1×1) low-energy electron-diffraction pattern indicates a well-ordered surface devoid of any reconstructions. The energy resolution was set to 9–11 and 15–20 meV for 18–35 and 35–90 eV photon energies, respectively, and the angular resolution was 0.35°. Additionally, an LSCO sample with $x = 0.01$ was measured at ALS with photon energy = 55 eV and $T = 20$ K.

3. Results

In figure 1, we present ARPES data taken at a photon energy of 27 eV. The dominant features in the angle-integrated spectrum are the valence band between 3.3 and 9 eV, an in-gap state near 1.3 eV and the QP peak at the Fermi level. The energy gap between the onset of the oxygen valence bands to the QP band bottom is around 3.3 eV, consistent with optical measurements [15], while local-density-approximation (LDA) band structure calculations predict a gap of ~ 2 eV [14, 16]. The presence of a non-dispersive and broad in-gap state around 1.3 eV has been discussed in the literature ([13] and references therein) as caused by a local screening effect, chemical disorder or donor levels.

Having established the basic spectral features, we now focus on the Fermi surface topography of STO. Figures 2(a)–(d) show ARPES data taken at various photon energies

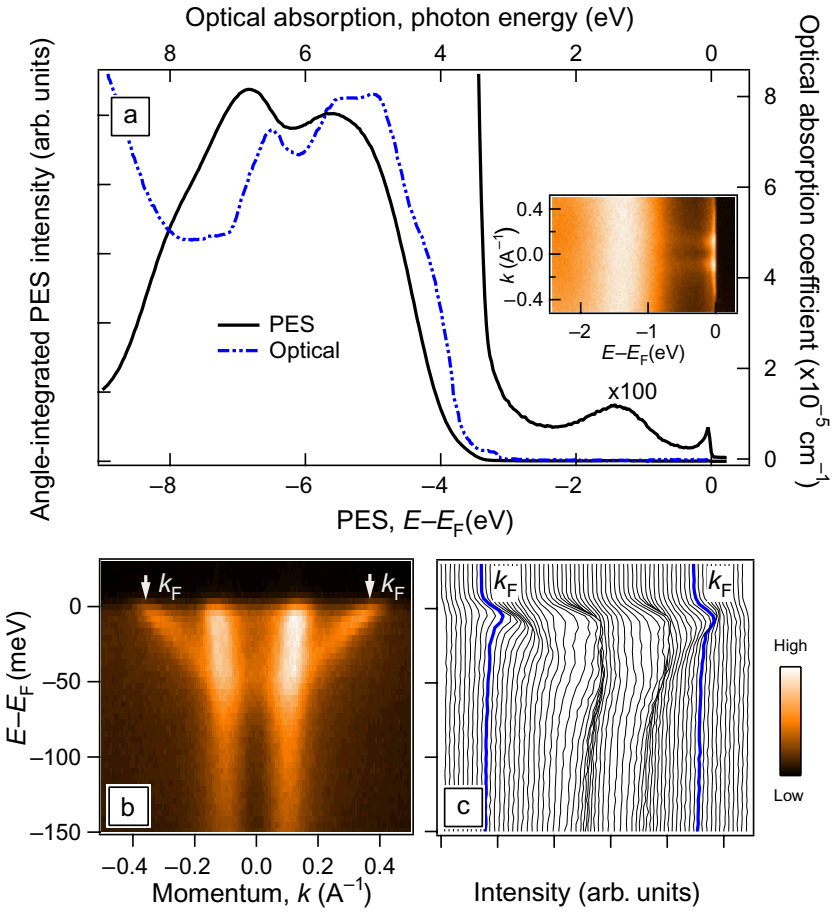

Figure 1. ARPES data of the $x = 0.01$ sample at $T = 10$ K. (a) Angle-integrated photoemission spectrum up to 9 eV in binding energy, together with optical absorption data of an undoped sample from [15]. The inset shows angle-resolved data of the in-gap state around 1.3 eV. (b) QP band dispersion in the (010) plane near E_F (see cut b in figure 2(f)) with corresponding energy distribution curves (EDCs) in (c).

(changing k_z) together with a Fermi surface map at 27 eV, projected on the k_x–k_y plane (figure 2(e)). The flatter band with an ∼60 meV band bottom (i.e. in figures 2(a)–(c)) corresponds to a bulk state since the k_F crossing changes with different photon energy (changing k_z), in agreement with LDA calculations by I I Mazin where the computational details are the same as in [11]. The steeper band with an ∼200 meV bottom (e.g. in figure 2(d)) can be attributed to the surface of cleaved STO because the data do not show noticeable dispersion along k_z and they are absent in LDA calculations (indicated by the blue line and surface in figures 2(e) and (f)). Since the surface band crosses the bulk band, it cannot be an eigenstate of the system but possibly a surface resonance state; this surface state is investigated further in smaller doping, $x = 0.001$ samples [17]. We also note that in $x = 0.01$ samples a second bulk band is expected with a Fermi crossing near the surface band. However, this band appears to be overshadowed by the more intense surface-related band and further suppressed by the matrix element near the Γ point. In the following, we will use the schematic contours of the k_F positions, indicated by green surfaces in figure 2(f), to describe the bulk Fermi surface.

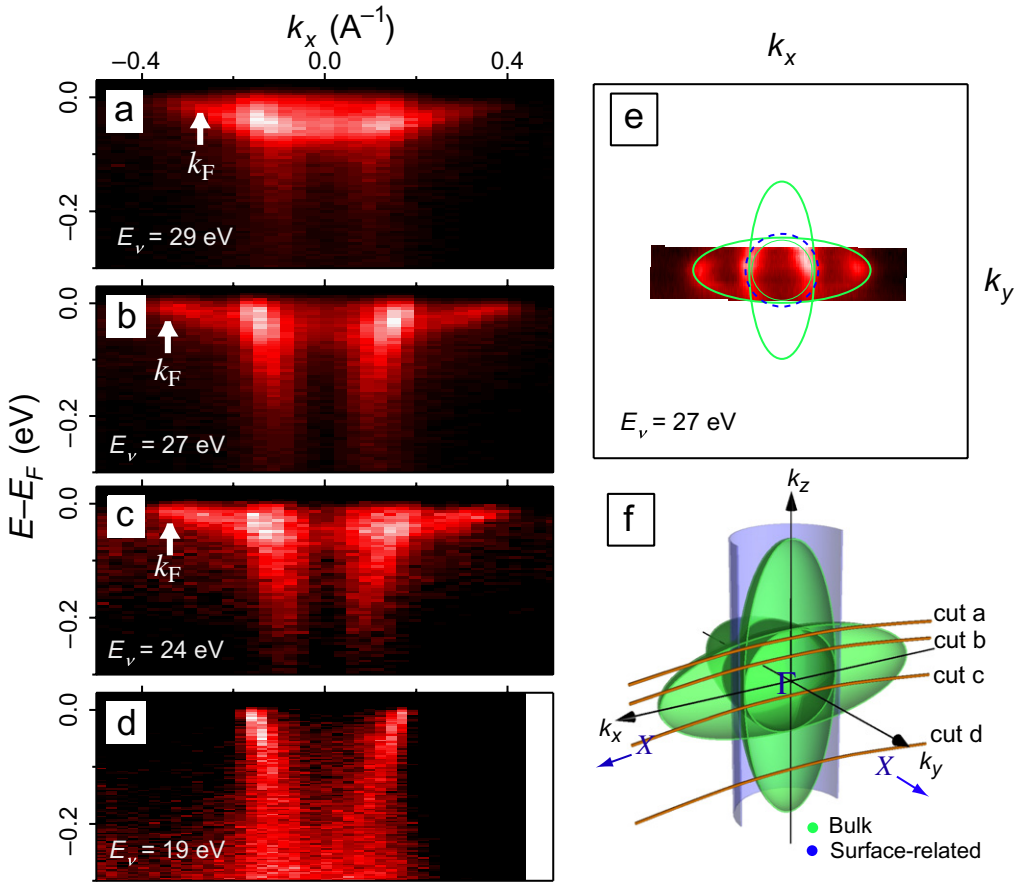

Figure 2. Fermi surface topography of STO. (a)–(d) Band dispersion in the (010) plane for photon energies of 19, 24, 27 and 29 eV, respectively. Doped STO has a cubic unit cell and a three-dimensional Fermi surface, consisting of three ellipsoid-like surfaces along each axis (see more details in [14]); when including the spin orbit coupling term in the calculation [11], a shift in the Fermi surface occurs, as shown in figure 3(e). (e) Fermi surface map near the Brillouin zone mid-plane ($h\nu = 27$ eV). The solid green lines are guides to the eye. Estimated k_z positions for (a)–(d) are indicated by the orange lines in the schematic Fermi surface (f), where half of the whole Fermi surface is plotted; green (blue) indicates the bulk (surface) band. Note that in $x = 0.01$ samples a second bulk band is expected with a Fermi crossing near the surface band. However, this band appears to be overshadowed by the more intense surface-related band and further suppressed by the matrix element near the Γ point.

Figures 3(a) and (b) show the occupied bands, along the ΓX direction in the vicinity of the Γ point of the $x = 0.01$ and 0.05 samples. By aligning the k_Fs of the ARPES data with those of the LDA dispersions [11], we estimate that the dopings of the $x = 0.01$ and 0.05 samples are slightly higher than the nominal dopings (1.5 ± 0.2 and 5.6 ± 0.5%, respectively: figure 3(e)), likely due to a small oxygen deficiency at the surface.

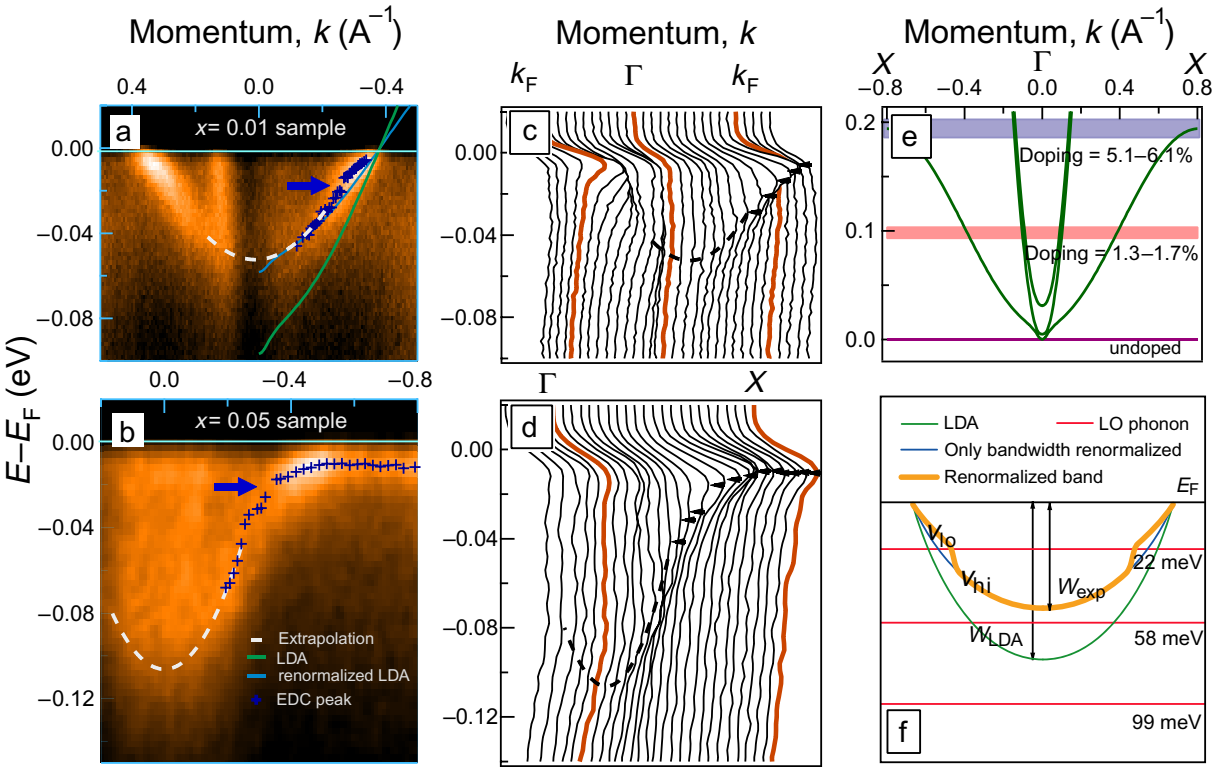

Figure 3. (a), (b) QP band dispersions of the $x = 0.01$ and 0.05 samples. Cross symbols indicate peaks from EDCs and dashed lines are extrapolated to obtain the band bottom. The most prominent kink energy is indicated by arrows around $\sim$20 meV for both doped samples. Possibly, there is a second kink in the $x = 0.05$ sample between 40 and 60 meV, but the complication from the side band makes it less clear. Note that k_z varies slightly along the k-axis of (a) and (b) (see figure 2). However, this change has only a minute influence on the measured group velocities and will be neglected for the discussion of mass renormalization. (c) and (d) show EDCs of ARPES data shown in (a) and (b), respectively, where the EDC peak positions are marked by triangle symbols and the dash lines are extrapolations. (e) LDA band dispersion of undoped STO along ΓX [11]. Fermi levels positions for dopings = 1.3–1.7 and 5.1–6.1% are indicated by shaded areas. (f) Schematic plot of renormalized band dispersion in the forms of 'kink' and reduced bandwidth caused by phonons whose mode energies are lower and higher than the electron bandwidth, respectively.

Having isolated the occupied part of the conduction bands (figures 3(a)–(d)), let us now turn to interpretation of the data. In the data one can discern a weak kink in the dispersion at approximately 20 meV binding energy (blue arrows, figures 3(a) and (b)). This is clear in the $x = 0.01$ sample, since in the $x = 0.05$ sample it resides in a region where the dispersion has a strong curvature (figure 3(e)). Such a weak kink structure in the dispersion indicates a perturbative coupling with a bosonic mode at this energy. This interpretation is supported by the observation that the intensity rapidly increases below the kink energy; above the kink energy, an extra decay channel that will smear the QP peak opens up. To quantify the coupling to

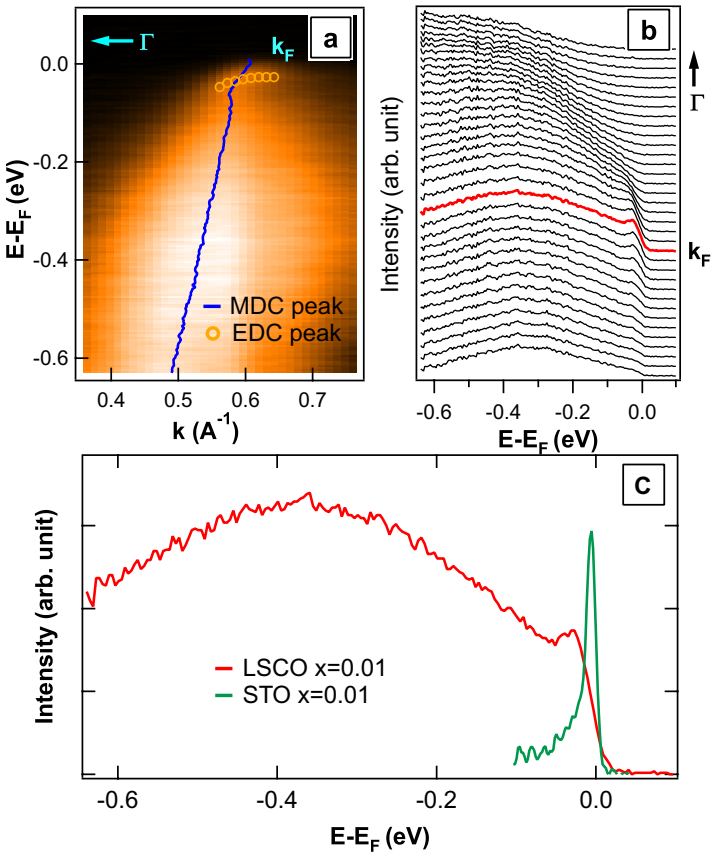

Figure 4. ARPES data of $La_{1-x}Sr_xCuO_4$ with $x = 0.01$. (a) Raw ARPES data; the blue line indicates the peak position in momentum distribution curves and orange circles indicate the peak positions in EDCs where the big arrow indicates the kink in dispersion at binding energy ∼70 meV. (b) Corresponding EDCs. (c) Comparison of ARPES spectra with background subtracted at k_F of (1) $x = 0.01$ STO sample along the $\Gamma - X$ direction and (2) 1% doping $La_{2-x}Sr_xCuO_4$ along the (0, 0) to (π, π) direction.

this boson, we extracted the band velocities for the $x = 0.01$ case at binding energies below (v_{lo}) and above (v_{hi}) the kink energy (see figure 3(f)) to be ∼0.16 and 0.21 eV Å, respectively. Mass renormalization is therefore $v_{hi}/v_{lo} = m^*/m \sim 1.3$, indicating a coupling to this particular boson, $\lambda' \equiv m^*/m - 1 = 0.3$.

Given that the signals are somewhat smeared at higher energies, we cannot exclude the presence of other kinks associated with higher energy modes. However, the data permit us to track the overall width of the occupied parts of the conduction bands. For the $x = 0.01$ sample we find the band bottom at ∼58 meV, whereas the LDA calculation indicates it to be at ∼97 meV [11] (figure 3(e)). It follows that the overall width of the occupied band is renormalized by a factor of ∼1.7 (W_{LDA}/W_{exp}). The total mass renormalization is the product of the bandwidth and kink renormalization factors and we find this to be $1.7 \times 1.3 \simeq 2.2$ in the $x = 0.01$ sample, close to the estimate 2–3 deduced from the optical measurements [11].

To compare with STO data, figure 4 shows ARPES data of $La_{1-x}Sr_xCuO_4$ with $x = 0.01$, as a lightly doped Mott insulator. The momentum is along the (0, 0) to (π, π) direction. We

note that all the data in figure 4 are already subtracted by the non-dispersive background of the oxygen valence band for clearer comparison. In contrast to STO, the spectrum (see the red line in figure 4(b)) shows a small QP peak with a large Frank–Condon-type broad hump around 400 meV—a signature of small-polaron formation. LSCO data also show a clear kink in the dispersion, indicating strong el–ph coupling at around 70 meV (see the arrow in figure 4(a)); to quantify this coupling, we extracted the band velocities at binding energies below ($v_{\rm lo}$) and above ($v_{\rm hi}$) the kink energy to be $\sim$1.66 and 6.14 eV Å, respectively. Therefore, the mass-renormalization factor from this kink feature is $v_{\rm hi}/v_{\rm lo} = m^*/m \sim 3.7$. The use of $\lambda' \equiv m^*/m - 1$ would give a λ' of 2.7, indicating a clear contrast to the extracted value of $\sim$0.3 from the kink feature of the $x = 0.01$ STO sample.

4. Discussion and conclusion

How does one interpret these findings from STO data? The 20 meV kink is certainly related to a phonon. *A priori* one can be less certain about the cause of overall bandwidth renormalization because an electronic origin cannot be excluded. However, although LDA is known to underestimate band gaps in band insulators, it does not usually underestimate the bandwidths and our extracted renormalization factor may be regarded as an upper value. At the same time, the phonon dispersions of STO have been measured by infrared and Raman spectroscopy [15] and neutron scattering [18]–[21] in great detail; the phonon modes are in the range of 0–100 meV where much of the phonon spectrum extends to energies that are larger than the Fermi energy of at least the $x = 0.01$ system. Under such an anti-adiabatic condition, one expects the el–ph coupling to give rise to an overall bandwidth renormalization that can be estimated from the mass-renormalization formulae for the isolated polaron [1]. Since the focus here is on the surprisingly moderate el–ph coupling, we attribute all the renormalization to el–ph interaction, which sets the upper bound for the value of $\lambda \sim 1$. An overall coupling $\lambda \sim 1$ can mean that small, self-trapped polarons are formed but also that the system stays itinerant. What decides the nomenclature is the length scale of the relevant el–ph couplings.

When the el–ph coupling is short ranged, small polarons are expected. One can take the cuprates as an example where an effective $\lambda \simeq 1$ corrected for electronic band narrowing effects [22] that enhance the impact of el–ph interaction is believed to be responsible for the multi-phonon Franck–Condon peak indicated in figure 4(c). Here we should note that m^* is no longer linear with λ and increases rapidly near the small-to-large polaron crossover around $\lambda \simeq 1$. For $\lambda \simeq 1$ in cuprates (e.g. in the case of LSCO shown in figure 4), the actual face value of mass renormalization could be as large as 3.7; hence, λ' defined by $m^*/m - 1$ would be 2.7.

The most striking aspect of the STO data is that such effects due to small-polaron formation are entirely absent in STO, where instead the electrons remain strongly coherent as manifested by the strong energy–momentum dispersion and the distinctly sharp QP peaks with large pole strengths even for the 1% doped sample (figure 4(c)). This can be reconciled with the relatively large λ, assuming that the dominating el–ph couplings are of the long-range, polar kind [23]. This claim can in fact be further substantiated by the finding that our data are in semi-quantitative agreement with 'naive' continuum limit estimations of the polar el–ph interactions [10, 24]. In this way, only the long-range electrostatic interactions are taken into account with the longitudinal optical (LO) phonons, omitting completely short-range interactions involving the transversal optical (TO) phonons that are, in reality, always present.

Table 1. Comparison of features between STO and cuprate—perovskite band and Mott insulators.

Feature	Mott insulator (La_2CuO_4)	Band insulator (STO)
Mass renormalization factor from the kink feature at small doping $x = 0.01$	∼3.7	∼1.3
Small polaronic effect at small doping	Yes	No
Large pseudogap behavior at small doping	Yes	No
Small Fermi surface pocket at small doping	Maybe (YBCO) [27]	Yes
Dielectric constant (undoped)	∼20 [28]	$\sim 10^2 - 10^4$

Starting from this perspective, let us first discuss why the large bulk dielectric constant may not be a good indicator for the formation of small polarons. The dielectric constants at zero frequency (ε_0) and at frequencies large by comparison to the phonon energy (ε_∞) are related to the frequencies of LO and TO phonons as $\varepsilon_0/\varepsilon_\infty = \Pi_a(\omega_{a\mathrm{LO}}/\omega_{a\mathrm{TO}})^2$, where a specifies the phonon branch. A large ε_0 signals a softening of the TO phonon that eventually can condense in a ferroelectric state. However, the Fröhlich polar el–ph interactions involve the LO phonons, where the large ε_0 will also help the coupling strength but with smaller effect. The coupling strength depends on the dielectric term $\kappa^{-1} = \varepsilon_\infty^{-1} - \varepsilon_0^{-1}$, which increases slightly upon increase of ε_0 ($\kappa^{-1} \sim 0.17$ in La_2CuO_4 and ∼0.19 in STO) [25]. Another issue is that the short-range coupling to this TO phonon could be enhanced due to the softening of the frequency ω_{TO}. However, since the softening occurs only in a narrow region in momentum space characterized by the scale $a/\xi \cong 0.1$ (ξ is the correlation length) [19, 20], the increase in the coupling constant $\Delta\lambda$ of the order of $\Delta\lambda \cong \lambda(\omega_{\mathrm{TO}}^0/\omega_{\mathrm{TO}})^2(a/\xi)^3$ is small.

Under these assumptions, one is, according to the calculations of Devreese *et al* [10, 24], left with three LO phonons at (for $q = 0$) 22, 58 and 99 meV with coupling constants α_i of 0.018, 0.945 and 3.090, respectively. Using that, for weak coupling, $\lambda_i = \alpha_i/6$ [1, 26] this translates into λ_i's of 0.003, 0.16 and 0.6, respectively. These modes are indicated together with the electronic dispersions in the schematic figure 3(f). The low-energy kink in the electron dispersions matches very well the 22 meV mode associated with Sr–O bond stretching [21]. The other two phonon modes are at higher energy than the band bottom and hence should cause an overall bandwidth reduction. For an accurate treatment, one may consider the anti-adiabatic limit; however from the available calculation, the coupling constants α of these 58 and 99 meV modes will give a bandwidth-renormalized factor of 1.76, which is already very close to our extracted value of ∼1.7. The polar el–ph calculation strongly underestimates the $\lambda' \simeq 0.3$ coupling to the 22 meV phonon. The main coupling from this Sr–O bond stretching mode comes from large momenta near the zone boundary as in the cuprates, and is expected

from general grounds due to the displacement eigenvectors. Thus, it is a local deformation. As discussed in the previous paragraph, this could well be significantly enhanced by proximity to the ferroelectric transition, one reason why its main impact is only on the low-energy phonon. However, given that the coupling is still moderate and this phonon is of the adiabatic/Eliashberg kind, it does not interfere with the consistency of our argument.

While small polarons are absent in STO, cuprates at similar doping show a sharp contrast in displaying strong el–ph coupling with mass renormalization as large as 3.7 (see table 1 for the comparison between LSCO and STO). For the following reasons, the carriers doped into a Mott insulator can be subject to a stronger short-range el–ph interaction. One reason is that the additional polaronic effect due to the magnetic degrees of freedom enhances the effective mass, and hence collaborate to form the composite small polaron with magnon and phonon clouds [29]. Another reason is that fluctuations with large momentum (e.g. $k = (\pi/2, \pi/2)$ of the antiferromagnetic state in the cuprates) are involved in dressing the doped carriers. Starting from the Fröhlich interaction, the exchange of this large momentum can lead to the short-range el–ph interaction. In the case of a band insulator, the large momentum in this same order of magnitude is not immediately available. Therefore, small-polaron formation is more likely to occur in a Mott insulator than in a band insulator. We should note that there could be an additional advantage in anisotropic layer compounds in that el–ph coupling along the perpendicular axis is little screened and hence remains strong [30, 31]. However, it is also known in cuprates that the small-polaron effect disappears largely upon doping away from the antiferromagnetism (e.g. $Na_xCa_{2-x}CuO_2Cl_2$ with $x = 0.12$ [3]), where the conductivity is still very anisotropic. Therefore, it is likely that there are also other physics (e.g. as discussed above) involved in helping the formation of small polarons.

In conclusion, we have shown the quite unexpected result that there is little evidence for small-polaron formation in lightly doped STO, indicating that the large dielectric behavior can occur independently of strong el–ph interactions. In turn, this indicates that in doped Mott insulators like the cuprates, the dressing of electrons by spin excitations [22, 29] and strong correlations combine to give a short-range el–ph interaction that is able to trap doped carriers and more readily form polarons.

Acknowledgments

We gratefully thank II Mazin for providing the unpublished LDA calculations, A Mishchenko for helpful discussion and H Takagi and J Matsuno for crystal information. This work was supported by the Department of Energy, Office of Basic Energy Sciences under contract DE-AC02-76SF00515. WM acknowledges The Thailand Research Fund for financial support. CCC was supported in part by National Science Council, Taiwan, under grant no. NSC-095-SAF-I-564-013-TMS.

References

[1] Devreese J T and Alexandrov A S 2009 *Rep. Prog. Phys.* **72** 066501
[2] Alexandrov A S and Mott N F 1994 *Rep. Prog. Phys.* **57** 1197
[3] Shen K M *et al* 2004 *Phys. Rev. Lett.* **93** 267002
[4] Yoshida T *et al* 2003 *Phys. Rev. Lett.* **91** 027001
[5] Mannella N *et al* 2005 *Nature* **438** 474

[6] Muller K A and Burkard H 1979 *Phys. Rev.* B **19** 3593
[7] Koonce C S *et al* 1967 *Phys. Rev.* **163** 380
[8] Suzuki H *et al* 1996 *Phys. J. Soc. Japan* **65** 1529
[9] Bednorz J G and Muller K A 1988 *Rev. Mod. Phys.* **60** 585
[10] Verbist G, Peeters F M and Devreese J T 1992 *Ferroelectrics* **130** 27
[11] Van Mechelen J L M *et al* 2008 *Phys. Rev. Lett.* **100** 226403
[12] Imada M, Fujimori A and Tokura Y 1998 *Rev. Mod. Phys.* **70** 1039
[13] Ishida Y *et al* 2008 *Phys. Rev. Lett.* **100** 056401
[14] Aiura Y *et al* 2002 *Surf. Sci.* **515** 61
[15] Cardona M 1965 *Phys. Rev.* A **140** 651
[16] Luo W *et al* 2004 *Phys. Rev.* B **70** 214109
[17] Meevasana W *et al* unpublished work
[18] Cowley R A 1964 *Phys. Rev.* A **134** 981
[19] Shirane G and Yamada Y 1969 *Phys. Rev.* **177** 858
[20] Shirane G 1974 *Rev. Mod. Phys.* **46** 437
[21] Choudhury N *et al* 2008 *Phys. Rev.* B **77** 134111
[22] Rosch O *et al* 2005 *Phys. Rev. Lett.* **95** 227002
[23] Toyozawa Y 2003 *Optical Processes in Solids* (Cambridge: Cambridge University Press) pp 149–87
[24] Eagles D M 1965 *Phys. J. Chem. Solids* **26** 672
[25] Alexandrov A S and Bratkovsky A M 2000 *Phys. Rev. Lett.* **84** 2043
[26] Feynman R P 1955 *Phys. Rev.* **97** 660
[27] Doiron-Leyraud N *et al* 2007 *Nature* **447** 565
[28] Tamasaku K *et al* 1992 *Phys. Rev. Lett.* **69** 1455
[29] Mishchenko A S and Nagaosa N 2004 *Phys. Rev. Lett.* **93** 036402
[30] Alexandrov A S 1996 *Phys. Rev.* B **53** 2863
[31] Meevasana W *et al* 2006 *Phys. Rev. Lett.* **96** 157003